

Resonant X-ray scattering and the $j_{\text{eff}} = 1/2$ electronic ground state in iridate perovskites

M. Moretti Sala,^{1,*} S. Boseggia,^{2,3} D. F. McMorrow,^{2,4} and G. Monaco¹

¹*European Synchrotron Radiation Facility, BP 220, F-38043 Grenoble Cedex, France*

²*London Centre for Nanotechnology and Department of Physics and Astronomy, University College London, London WC1E 6BT, United Kingdom*

³*Diamond Light Source Ltd, Diamond House, Harwell Science and Innovation Campus, Didcot, Oxfordshire OX11 0DE, United Kingdom*

⁴*Department of Physics, Technical University of Denmark, DK-2800 Kgs. Lyngby, Denmark*

The resonant X-ray scattering (magnetic elastic, RXMS, and inelastic, RIXS) of Ir^{4+} at the $L_{2,3}$ edges relevant to spin-orbit Mott insulators $\text{A}_{n+1}\text{Ir}_n\text{O}_{3n+1}$ ($\text{A}=\text{Sr}, \text{Ba}, \text{etc.}$) are calculated using a single-ion model which treats the spin-orbit and tetragonal crystal-field terms on an equal footing. Both RXMS and RIXS in the spin-flip channel are found to display a non-trivial dependence on the direction of the magnetic moment, $\boldsymbol{\mu}$. Crucially, we show that for $\boldsymbol{\mu}$ in the ab -plane, RXMS at the L_2 edge is zero *irrespective* of the tetragonal crystal-field; spin-flip RIXS, relevant to measurements of magnons, behaves reciprocally being zero at L_2 when $\boldsymbol{\mu}$ is perpendicular to the ab -plane. Our results provide important insights into the interpretation of X-ray data from the iridates, including that a $j_{\text{eff}} = 1/2$ ground state cannot be assigned on the basis of L_2/L_3 intensity ratio alone.

The existence of a Mott-like insulating ground state for specific members of the Ruddlesden-Popper series of iridate perovskites $\text{A}_{n+1}\text{Ir}_n\text{O}_{3n+1}$ ($\text{A}=\text{Sr}, n = 1, 2; \text{A}=\text{Ba}, n = 1; \text{A}=\text{Ca}, n = \infty$) has stimulated intense interest[1–7]. Common wisdom had held that metallic ground states should be displayed ubiquitously by 5d compounds due to the weakening of the onsite Coulomb repulsion, U , and the broadening of the bandwidth, W , both resulting from the extended nature of the 5d orbitals. It has been proposed, however, that for Ir^{4+} ($5d^5$) the strong spin-orbit coupling (SOC) present produces a $j_{\text{eff}} = 1/2$ groundstate upon which even a moderate U can act to open a gap, hence leading to the formation of an insulating state[1, 2]. While such spin-orbit Mott insulators are of interest in their own right, further impetus for their study comes from their structural similarities to certain cuprates, and not least the prediction that they may form new families of superconductors[8, 9].

Since the $j_{\text{eff}} = 1/2$ groundstate is actually an idealisation – realised in perfect cubic symmetry only – of pivotal importance is the need to understand the robustness of this state to non-cubic structural distortions found in real materials. This issue has been addressed through various experimental probes, including optical absorption, angle-resolved photo emission, X-ray absorption, etc.[1, 2] One technique that has played a particularly prominent role in this endeavour is resonant X-ray magnetic scattering (RXMS), following the seminal work of Kim et al.[3] on Sr_2IrO_4 who argued that the near vanishing of the RXMS intensity at the L_2 edge first observed in their experiments was directly related to the existence of a $j_{\text{eff}} = 1/2$ ground state. Although doubts have been raised concerning this interpretation[5, 10], others have followed the spirit of Kim et al. and invoked the L_2/L_3 RXMS intensity ratio as a proxy for the full understanding of the electronic structure[6, 7, 11–14].

This has led to some unexpected conclusions, including the fact that a $j_{\text{eff}} = 1/2$ groundstate is apparently realised in Ba_2IrO_4 [7] even though the IrO_6 octahedra have a tetragonal distortion almost twice as large as that in Sr_2IrO_4 [15]. Moreover, in bilayer $\text{Sr}_3\text{Ir}_2\text{O}_7$ the magnetic moments undergo an unusual reorientation transition to point perpendicular to the basal plane order displayed by the $n = 1$ “214” counterparts while at the same time they display a L_2/L_3 RXMS intensity ratio no larger than that of the $n = 1$ compounds[12, 13, 16].

There is thus a clear need to elucidate fully the relationship between the L_2/L_3 RXMS intensity ratio, the direction of the magnetic moment, and the presence or otherwise of a $j_{\text{eff}} = 1/2$ ground state. To this end we utilise a single-ion model which allows us to treat the SOC ζ and a tetragonal crystal field Δ on an equal footing[6, 17–19]. This model has been chosen for the direct physical insight it provides. We use it to explore both RXMS, and the RIXS in the spin-flip channel. This latter channel has recently been exploited in various iridates to yield full magnon dispersion curves across the entire Brillouin zone[20, 21]: information that was previously the exclusive province of neutron spectroscopy. We focus in particular on the explicit dependence of the X-ray scattering on the direction of the local Ir^{4+} magnetic moment, $\boldsymbol{\mu}$. Realistic values of ζ and Δ are chosen to aid comparison with experimental data[18, 22]. Our main finding is that both the RXMS and RIXS in the spin-flip channel display a non-trivial dependence on the direction of $\boldsymbol{\mu}$. We show that the L_2 edge RXMS intensity is identically zero for magnetic moments lying in the ab -plane, *irrespective* of the tetragonal crystal field splitting of the t_{2g} states, in agreement with the symmetry arguments of Ref. [10]. This has the important consequence that RXMS cannot be used in isolation to deduce the existence or otherwise of the $j_{\text{eff}} = 1/2$ groundstate, calling for a reinterpretation

tion of RXMS data on the $A_2\text{IrO}_4$ ($A=\text{Sr}$ and Ba) compounds for which the magnetic moments are known to lie in the ab -plane[3, 7]. Our results are discussed with reference to existing experimental data, and consideration given to their implications for future work.

The calculation method adopted here for Ir^{4+} follows along similar lines to that in Refs. 23 and 24 for $L_{2,3}$ edge RIXS in Cu^{2+} cuprates (one-hole e_g systems). For Ir^{4+} we limit ourselves to the subspace of t_{2g} states, setting aside the e_g states, justified by the large octahedral crystal field splitting ($10Dq \sim 1-10$ eV), which for the $5d^5$ configuration of Ir^{4+} produces a single hole in the t_{2g} states, and the hierarchy of energy-scales at play, $\Delta \ll \zeta \ll 10Dq$. Iridates can thus be thought of as one-hole t_{2g} systems: dealing with one-particle systems greatly simplifies the calculations, as particle-particle interactions are zeroed, and expressions for one-particle ground and excited states wavefunctions are readily derived. Resonant X-ray scattering amplitudes are then calculated considering intra-ion transitions. The assumption of considering the subspace spanned by the t_{2g} states only is further justified by the observation in Ir L_3 edge RXMS and RIXS that the magnetic elastic and magnetic and spin-orbit excitations resonate at $\sim 10Dq$ lower energy than the main absorption line[11, 18], indicating that they originate from initial $2p \rightarrow 5d$ transitions into the same unoccupied states within the Ir t_{2g} manifold[18].

The Hamiltonian acting on the $5d$ t_{2g} states relevant to iridate perovskites is written as[6, 17–19]

$$\mathcal{H} = \zeta \mathbf{L} \cdot \mathbf{S} - \Delta \langle L_z \rangle^2. \quad (1)$$

For negligible SOC ($\zeta = 0$), its eigenstates are the familiar $|xy, \pm\rangle$, $|yz, \pm\rangle$ and $|zx, \pm\rangle$ orbitals, where \pm refers to the spin. In the case of iridium, however, SOC can be as large as 0.45 eV[25], and therefore cannot be neglected. For negligible tetragonal crystal-field, i.e. for $\Delta = 0$, the groundstate of the system is the so-called $|j_{\text{eff}} = 1/2\rangle$ state described below. At intermediate couplings, the eigenstates of \mathcal{H} are three Kramers doublets, which we write as $|0, \pm\rangle$, $|1, \pm\rangle$ and $|2, \pm\rangle$.

An essential pre-requisite for calculating the resonant X-ray scattering amplitudes is to determine the eigenvalues and eigenfunctions of Eq.(1), which for completeness we present here. The eigenvalues (see Supplementary Materials) are shown in Fig.1(a) for $\zeta = 0.45$ eV (as extracted from experiments[18, 22, 26]) and realistic values of Δ , i.e $|\Delta| < 1$ eV[18, 19, 22]. With five electron filling the three doublets, one hole is left in the, say, $|0, -\rangle$ state, which is therefore the ground state of the system in the *hole* representation. The corresponding wavefunction is written as

$$|0, -\rangle_c = \frac{C_0 |xy, -\rangle + |yz, +\rangle - \nu |zx, +\rangle}{\sqrt{2 + C_0^2}} \quad (2)$$

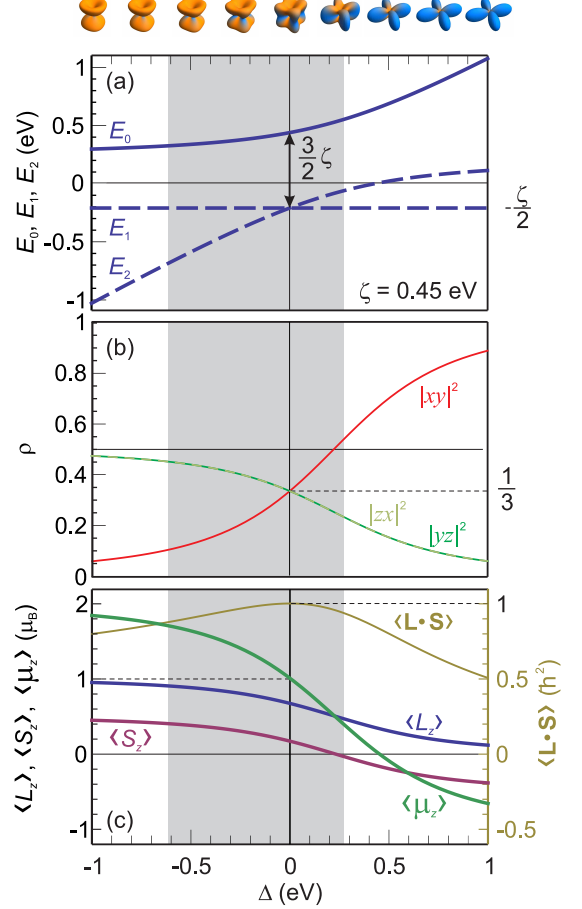


FIG. 1. Δ dependence of (a) eigenvalues of Eq.(1) (blue lines), (b) the groundstate orbital occupancies of the $|xy, -\rangle$ (red), $|yz, +\rangle$ (green) and $|zx, +\rangle$ (yellow line) states, and (c) the expectation values of the orbital ($\langle L_z \rangle$, blue), spin ($\langle S_z \rangle$, purple) and total ($\langle \mu_z \rangle$, green) magnetic moment components along z , and expectation value of the angular part of the spin orbit coupling ($\langle \mathbf{L} \cdot \mathbf{S} \rangle$, yellow line). The continuous blue line in panel (a) represent the ground state energy in the *hole* representation. The corresponding wavefunction (according to Eq.(2)) is represented at the top: blue and orange represent the contributions of the $|xy, -\rangle$ and $(|yz, +\rangle - \nu |zx, +\rangle) / \sqrt{2}$ states, respectively. The shaded area in all panels represents the range of Δ values, for which the L_2/L_3 RXMS intensity ratio is smaller than 0.1 (see Fig.2).

for $\boldsymbol{\mu} \parallel (001)$, and

$$|0, -\rangle_{ab} = \frac{C_0 (|xy, -\rangle - \nu |xy, +\rangle) / \sqrt{2} + |yz, +\rangle + \nu |zx, -\rangle}{\sqrt{2 + C_0^2}} \quad (3)$$

for $\boldsymbol{\mu} \parallel (110)$, respectively, where $2C_0 = \delta - 1 + \sqrt{9 + \delta(\delta - 2)}$ and $\delta = 2\Delta/\zeta$. We mostly focus on $\boldsymbol{\mu} \parallel (001)$ and $\boldsymbol{\mu} \parallel (110)$, as these are the cases for $\text{Sr}_3\text{Ir}_2\text{O}_7$ and A_2IrO_4 ($A=\text{Sr}$ and Ba), respectively. For

$\Delta = \delta = 0$ ($C_0 = 1$), the $j_{\text{eff}} = 1/2$ ground state is realized, and Eqs.(2) and (3) reduce to

$$|j_{\text{eff}} = \frac{1}{2}\rangle_c = \frac{|xy, -\rangle + |yz, +\rangle - \iota|zx, +\rangle}{\sqrt{3}} \quad (4)$$

and

$$|j_{\text{eff}} = \frac{1}{2}\rangle_{ab} = \frac{(|xy, -\rangle - \iota|xy, +\rangle)/\sqrt{2} + |yz, +\rangle + \iota|zx, -\rangle}{\sqrt{3}} \quad (5)$$

respectively. It has to be stressed here that the expression of $|j_{\text{eff}} = 1/2\rangle$ is different in the two cases $\boldsymbol{\mu} \parallel (001)$ and $\boldsymbol{\mu} \parallel (110)$.

At the top of Fig.1, a real-space representation is given of $|0, -\rangle$ as a function of Δ : the well-known ‘‘cubic’’ shape of the $|j_{\text{eff}} = 1/2\rangle$ wavefunction is evident for $\Delta = 0$. At finite values of Δ , the admixture of orbital contributions changes: in particular, in the limit for $\Delta \gg \zeta$, the ground state reduces to the $|xy, -\rangle$, while it reads $(|yz, +\rangle - \iota|zx, +\rangle)/\sqrt{2}$ for $\Delta \ll -\zeta$. This is also seen in Fig.1(b), where the relative orbital occupancy is shown: this is the same for the three orbitals, i.e. $(1/\sqrt{3})^2 = 1/3$, at $\Delta = 0$. Fig.1(c), finally, shows the Δ dependence of the expectation values of the orbital ($\langle L_z \rangle$, blue), spin ($\langle S_z \rangle$, purple) and total ($\langle \mu_z \rangle$, green) magnetic moment components along z , for $\boldsymbol{\mu} \parallel (001)$. Note that $\langle \mu_z \rangle = 1$ for $\Delta = 0$ and $\langle \mu_z \rangle = 0$ for $\Delta = \zeta$. The Δ dependence of the expectation value of the spin orbit coupling operator ($\langle \mathbf{L} \cdot \mathbf{S} \rangle$, yellow line), independent of the magnetic moment orientation, is also shown to reach a maximum of 1 at $\Delta = 0$, as expected. (See Supplementary Materials for the expression of the expectation values of the momentum and spin-orbit operators for both $\boldsymbol{\mu} \parallel (001)$ and (110)).

Having obtained the eigenvalues and eigenfunctions of Eq.(1) we now proceed to the main task of calculating the required resonant X-ray scattering amplitudes. RIXS is a second-order process described by the Kramers-Heisenberg (KH) formula:

$$\mathcal{A}_{|f, \pm\rangle}^{\epsilon \epsilon'} = \sum_n \frac{\langle f, \pm | \mathcal{D}_{\epsilon'}^\dagger | n \rangle \langle n | \mathcal{D}_\epsilon | 0, - \rangle}{E_0 - E_n + \hbar\omega + \iota\Gamma_n} \quad (6)$$

is the scattering amplitude from the ground state, $|0, -\rangle$ (of energy E_0) to the final states $|f, \pm\rangle$ ($f = 0, 1, 2$, energy E_f). n runs over all the intermediate states of energy E_n and intrinsic linewidth Γ_n . \mathcal{D}_ϵ ($\mathcal{D}_{\epsilon'}^\dagger$) is the absorption (emission) transition operator, where ϵ (ϵ') defines the polarisation of the incoming (outgoing) photons. At resonance ($\hbar\omega \approx E_0 - E_n$), this is the leading term in the RIXS cross-section and the only one considered here. Assuming that, at a given edge ($E_n = E$), the intermediate states have all the same intrinsic linewidth $\Gamma_n = \Gamma$, the denominator of Eq.(6) can be discarded, and the expression of the atomic form factor simplifies to $\mathcal{A}_{|f, \pm\rangle}^{\epsilon \epsilon'} \propto \sum_n \langle f, \pm | \mathcal{D}_{\epsilon'}^\dagger | n \rangle \langle n | \mathcal{D}_\epsilon | 0, - \rangle$.

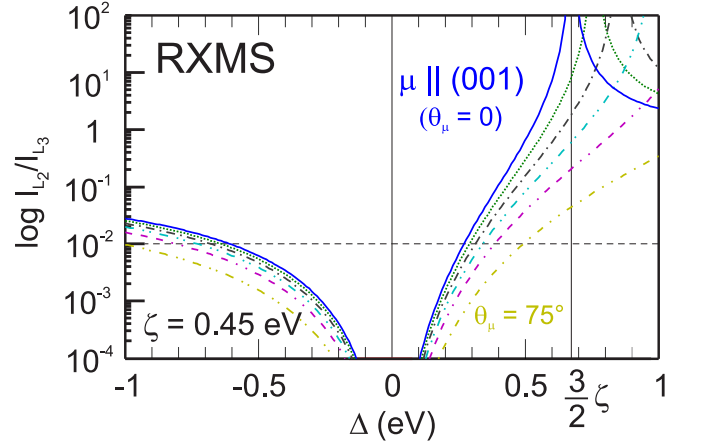


FIG. 2. L_2/L_3 RXMS intensity ratio (logarithmic scale) as a function of the tetragonal crystal field splitting Δ ranging from -1 to 1 eV, for a given value of the SOC constant ($\zeta = 0.45$ eV). Different line styles correspond to values of θ_μ from 0 to 90° in steps of 15° .

To calculate the matrix elements of the resonant scattering amplitudes, we use the atomic wavefunctions derived within the single ion model, and restrict ourselves to the case of dipolar transitions. The scattering geometry (sketched in the Supplementary Materials) is defined through the azimuthal, θ (θ'), and polar, ϕ (ϕ'), angles of the incident (scattered) photon wavevector, \mathbf{k} (\mathbf{k}'), in the sample reference system. The polarisation ϵ (ϵ') of the incident (scattered) photon is projected on a two-vector basis, perpendicular (σ) and parallel (π) to the scattering plane.

The resonant elastic X-ray scattering amplitude (REXS) is obtained in the special case that $|f, \pm\rangle \equiv |0, -\rangle$. For a crystal, the REXS cross-section in general is proportional to $|\mathcal{F}^{\epsilon \epsilon'}(\mathbf{Q})|^2$, where $\mathcal{F}^{\epsilon \epsilon'}(\mathbf{Q})$ is the unit cell structure factor, and $\mathbf{Q} = \mathbf{k}' - \mathbf{k}$. For the specific case of antiferromagnetic order considered here, the RXMS structure factor is derived as a sum over two sub lattices (A and B , say), so that

$$\mathcal{F}^{\epsilon \epsilon'}(\mathbf{Q}) = f_A^{\epsilon \epsilon'} \sum_A e^{i\mathbf{Q} \cdot \mathbf{r}_A} + f_B^{\epsilon \epsilon'} \sum_B e^{i\mathbf{Q} \cdot \mathbf{r}_B}, \quad (7)$$

with $f_A^{\epsilon \epsilon'} = \mathcal{A}_{|0, -\rangle}^{\epsilon \epsilon'}$, \mathbf{r}_A (\mathbf{r}_B) the position of the A (B) atom within the magnetic unit cell, and $\mathbf{Q} = \mathbf{Q}_{AF}$, the antiferromagnetic propagation wavevector.

We now consider the RXMS intensity branching ratio, $|\mathcal{F}_{L_2}^{\sigma\pi}|^2 / |\mathcal{F}_{L_3}^{\sigma\pi}|^2$, as this is the quantity, readily measured in experiments, which has been used to infer the existence of a $j_{\text{eff}} = 1/2$ ground state in various iridate perovskites. With $\boldsymbol{\mu} \parallel (001)$ the REXS scattering amplitudes at the L_2 edge are given by $\mathcal{A}_{|0, -\rangle}^{\sigma\pi} = \iota(C_0 - 1)^2 \cos \theta' / (2 + C_0^2)$ and $\mathcal{A}_{|0, -\rangle}^{\pi\sigma} = -\iota(C_0 - 1)^2 \cos \theta' / (2 + C_0^2)$, while at the L_3 edge these read $\mathcal{A}_{|0, -\rangle}^{\sigma\pi} = -\iota[C_0(C_0 - 2) - 2] \cos \theta' / (2 + C_0^2)$ and

$\mathcal{A}_{|0,-\rangle}^{\pi\sigma} = i[C_0(C_0 - 2) - 2] \cos\theta / (2 + C_0^2)$. Given the scattering amplitudes and the atomic positions within the unit cell, the RXMS intensity branching ratio is given by

$$\frac{|\mathcal{F}_{L_2}^{\sigma\pi}|^2}{|\mathcal{F}_{L_3}^{\sigma\pi}|^2} = \frac{|\mathcal{F}_{L_2}^{\pi\sigma}|^2}{|\mathcal{F}_{L_3}^{\pi\sigma}|^2} = \frac{(C_0 - 1)^4}{[C_0(C_0 - 1) - 2]^2} \quad (8)$$

Its dependence on the tetragonal distortion is shown in Fig.2 (blue curve) for $\zeta = 0.45$ eV, and is consistent with previous calculations with $\boldsymbol{\mu} \parallel (001)$ [20], relevant to the case of $\text{Sr}_3\text{Ir}_2\text{O}_7$. The calculated branching ratio drops to zero for $\Delta = 0$, while it diverges for $\Delta = 3\zeta/2$. In the limit for $\Delta \gg \zeta$, the ratio tends to unity, and to $1/4$ for $\Delta \ll -\zeta$. It was claimed that the experimental ratio of at most 1% provides the lower and upper bounds for nearly pure $j_{\text{eff}} = 1/2$ ground state. We note, however, that these bounds correspond to a relatively large energy window in Δ (-0.61 eV $< \Delta < 0.27$ eV), for which the ground state may deviate considerably from the pure $j_{\text{eff}} = 1/2$ state, as seen in the substantial change of the shape of the ground state wavefunction, of the orbital occupancy ($0.1 < |xy|^2 < 0.54$), and of the expectation values of $\langle L_z \rangle$, $\langle S_z \rangle$ and $\langle \mathbf{L} \cdot \mathbf{S} \rangle$ (Fig.1). Nonetheless, the experimentally observed branching ratio in $\text{Sr}_3\text{Ir}_2\text{O}_7$ is less than 1%, and it is probably reasonable to conclude that in this case the RXMS experiments provide evidence of a $j_{\text{eff}} = 1/2$ ground state.

Figure 2 also shows the dependence of the RXMS branching ratio on the direction of $\boldsymbol{\mu}$, defined through the θ_μ angle ($\boldsymbol{\mu} \parallel (001)$ for $\theta_\mu = 0$, while $\boldsymbol{\mu} \parallel (110)$ for $\theta_\mu = 90^\circ$). When $\boldsymbol{\mu}$ is progressively lowered into the basal plane, the divergence in the ratio moves towards higher values of Δ , and eventually disappears for $\theta_\mu = 90^\circ$. Consequently, for magnetic moments lying in the ab -plane, the L_2 edge RXMS intensity is identically zero, *irrespective* of the tetragonal crystal field splitting of the t_{2g} states. (This can be traced to the fact that for $\boldsymbol{\mu} \parallel (110)$, $\mathcal{A}_{|0,-\rangle}^{\sigma\pi} = \mathcal{A}_{|0,-\rangle}^{\pi\sigma} \equiv 0$, a consequence of the particular coherent superposition of states in Eq.(5)). This is an important result as it implies that the $j_{\text{eff}} = 1/2$ ground state cannot be inferred by the L_2/L_3 RXMS intensity ratio when $\boldsymbol{\mu} \perp (110)$, as has been claimed in the case of A_2IrO_4 (A=Sr, Ba) compounds[3, 7].

We have also calculated the RIXS amplitudes associated with transitions to excited states within the 5d t_{2g} manifold. Here we focus on the “spin-flip” channel from the $|0, -\rangle$ ground state to the $|0, +\rangle$ final state, pertinent to the interpretation of experiments that have successfully observed magnons. In Fig.3 we report the L_2/L_3 “spin-flip” intensity ratio as a function of Δ (for $\zeta = 0.45$ eV). Remarkably, it is seen that the dependence on the direction of $\boldsymbol{\mu}$ is opposite to that of RXMS: the ratio is identically zero for magnetic moments along the c -axis, irrespective of the tetragonal crystal field splitting, while for all other $\boldsymbol{\mu}$ orientations it drops to zero only for $\Delta = 0$,

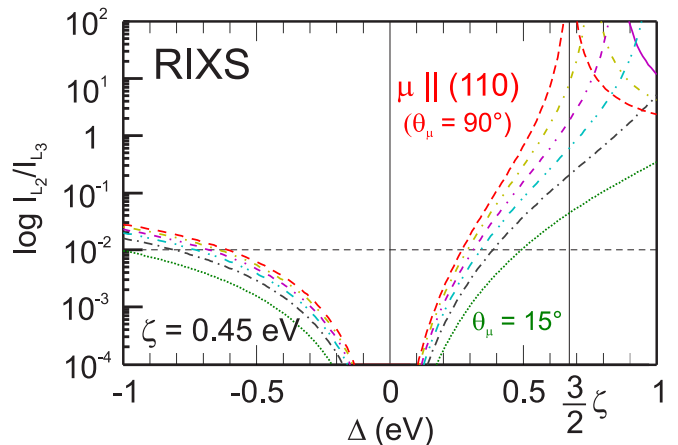


FIG. 3. Ratio of the L_2/L_3 “spin-flip” intensity ratio (logarithmic scale) as a function of the tetragonal crystal field splitting Δ ranging from -1 to 1 eV, for a given value of the SOC constant ($\zeta = 0.45$ eV). Different line styles correspond to values of θ_μ from 90 to 0° in steps of 15° .

i.e. when the $j_{\text{eff}} = 1/2$ ground state is realized.

It remains to consider the extent to which the salient results of our calculations may be altered by the inclusion of additional effects, such as the e_g states, electronic band formation, many-body interactions, etc. Although these will all no doubt affect the quantitative dependences on θ_μ and Δ shown in Figs. 2 and 3, we nevertheless expect the qualitative features of our results to remain unchanged. The reason is that ultimately, effects such as the extinguishing of the RXMS L_2 intensity for $\theta_\mu = 90^\circ$, depends on the symmetry of the 5d wave function which partially persists into the solid. When comparing with the results of RXMS experiments, it should be appreciated that with the limited energy resolution usually employed (~ 1 eV) what is actually measured is the sum of elastic plus partially integrated inelastic responses. Thus the differences exhibited by the Sr and Ba “214” compounds – the L_2 intensity being small and finite in the former and zero in the latter – could be related to the detailed differences of the excitation spectra for the two systems.

In conclusion, we have developed a single-ion model relevant to the iridate perovskites by which we are able to understand how the results of resonant X-ray elastic and inelastic scattering experiments relate to their underlying electronic structure. Our model treats the SOC, ζ , and tetragonal crystal field, Δ , on an equal footing and, most importantly, explicitly takes into account the direction θ_μ of the Ir^{4+} magnetic moments, $\boldsymbol{\mu}$. The results of our calculations reveal the full complexity of the relationship between ζ , Δ and θ_μ in determining the RXMS and RIXS cross-sections at the L_2 and L_3 edges. In terms of existing experimental data[3, 6, 7], our results clearly call for a reinterpretation as the L_2 RXMS cross-section is zero for $\theta_\mu = 90^\circ$ irrespective of the value of Δ . Our

calculations will also be useful in guiding future experiments, including, for example, the properties of thin films of iridates have started to be explored[27, 28]. Here the strong magneto-elastic coupling inherent to the iridates might allow epitaxial strain effects to be used to control magnetic structure, including moment reorientation transitions, etc. According to our calculations, any such transitions will have a clear signature in the RXMS and RIXS intensity ratios. Finally, although the focus here has been on iridate perovskites, the general approach we have developed can be readily extended to other systems of interest.

Acknowledgments - The authors would like to acknowledge F. de Bergevin, L. Braicovich, G. Ghiringhelli and C. Mazzoli for stimulating and elucidating discussions. The work in the UK was supported through a grant from the EPSRC, and in Denmark by the Nordea Fonden and the Otto Mønstedts Fond.

* marco.moretti@esrf.fr

- [1] B. J. Kim, H. Jin, S. J. Moon, J. Kim, B. Park, C. S. Leem, J. Yu, T. W. Noh, C. Kim, S. Oh, J. Park, V. Durairaj, G. Cao, and E. Rotenberg, *Physical Review Letters* **101**, 076402 (2008).
- [2] S. J. Moon, H. Jin, K. W. Kim, W. S. Choi, Y. S. Lee, J. Yu, G. Cao, A. Sumi, H. Funakubo, C. Bernhard, and T. W. Noh, *Physical Review Letters* **101**, 226402 (2008).
- [3] B. J. Kim, H. Ohsumi, T. Komesu, S. Sakai, T. Morita, H. Takagi, and T. Arima, *Science* **323**, 1329 (2009).
- [4] G. Jackeli and G. Khaliullin, *Phys. Rev. Lett.* **102**, 017205 (2009).
- [5] D. Haskel, G. Fabbri, M. Zhernenkov, P. P. Kong, C. Q. Jin, G. Cao, and M. van Veenendaal, *Phys. Rev. Lett.* **109**, 027204 (2012).
- [6] K. Ohgushi, J.-i. Yamaura, H. Ohsumi, K. Sugimoto, S. Takeshita, A. Tokuda, H. Takagi, M. Takata, and T.-h. Arima, *Phys. Rev. Lett.* **110**, 217212 (2013).
- [7] S. Boseggia, R. Springell, H. C. Walker, H. M. Rønnow, C. Rüegg, H. Okabe, M. Isobe, R. S. Perry, S. P. Collins, and D. F. McMorrow, *Phys. Rev. Lett.* **110**, 117207 (2013).
- [8] H. Watanabe, T. Shirakawa, and S. Yunoki, *Physical Review Letters* **105**, 216410 (2010).
- [9] F. Wang and T. Senthil, *Physical Review Letters* **106**, 136402 (2011).
- [10] L. C. Chapon and S. W. Lovesey, *Journal of Physics: Condensed Matter* **23**, 252201 (2011).
- [11] S. Boseggia, R. Springell, H. C. Walker, A. T. Boothroyd, D. Prabhakaran, D. Wermeille, L. Bouchenoire, S. P. Collins, and D. F. McMorrow, *Phys. Rev. B* **85**, 184432 (2012).
- [12] S. Boseggia, R. Springell, H. C. Walker, A. T. Boothroyd, D. Prabhakaran, S. P. Collins, and D. F. McMorrow, *Journal of Physics: Condensed Matter* **24**, 312202 (2012).
- [13] J. W. Kim, Y. Choi, J. Kim, J. F. Mitchell, G. Jackeli, M. Daghofer, J. van den Brink, G. Khaliullin, and B. J. Kim, *Phys. Rev. Lett.* **109**, 037204 (2012).
- [14] S. Calder, G.-X. Cao, M. D. Lumsden, J. W. Kim, Z. Gai, B. C. Sales, D. Mandrus, and A. D. Christianson, *Phys. Rev. B* **86**, 220403 (2012).
- [15] H. Okabe, M. Isobe, E. Takayama-Muromachi, A. Koda, S. Takeshita, M. Hiraishi, M. Miyazaki, R. Kadono, Y. Miyake, and J. Akimitsu, *Physical Review B* **83**, 155118 (2011).
- [16] S. Fujiyama, K. Ohashi, H. Ohsumi, K. Sugimoto, T. Takayama, T. Komesu, M. Takata, T. Arima, and H. Takagi, *Phys. Rev. B* **86**, 174414 (2012).
- [17] L. J. P. Ament, G. Khaliullin, and J. van den Brink, *Physical Review B* **84**, 020403 (2011).
- [18] X. Liu, V. M. Katukuri, L. Hozoi, W.-G. Yin, M. P. M. Dean, M. H. Upton, J. Kim, D. Casa, A. Said, T. Gog, T. F. Qi, G. Cao, A. M. Tsvetlik, J. van den Brink, and J. P. Hill, *Phys. Rev. Lett.* **109**, 157401 (2012).
- [19] L. Hozoi, H. Gretarsson, J. P. Clancy, B.-G. Jeon, B. Lee, K. H. Kim, V. Yushankhai, P. Fulde, Y.-J. Kim, and J. van den Brink, *ArXiv e-prints* (2012), arXiv:1212.4009 [cond-mat.str-el].
- [20] J. Kim, D. Casa, M. H. Upton, T. Gog, Y.-J. Kim, J. F. Mitchell, M. van Veenendaal, M. Daghofer, J. van den Brink, G. Khaliullin, and B. J. Kim, *Phys. Rev. Lett.* **108**, 177003 (2012).
- [21] J. Kim, A. H. Said, D. Casa, M. H. Upton, T. Gog, M. Daghofer, G. Jackeli, J. van den Brink, G. Khaliullin, and B. J. Kim, *Phys. Rev. Lett.* **109**, 157402 (2012).
- [22] H. Gretarsson, J. P. Clancy, X. Liu, J. P. Hill, E. Bozin, Y. Singh, S. Manni, P. Gegenwart, J. Kim, A. H. Said, D. Casa, T. Gog, M. H. Upton, H.-S. Kim, J. Yu, V. M. Katukuri, L. Hozoi, J. van den Brink, and Y.-J. Kim, *Phys. Rev. Lett.* **110**, 076402 (2013).
- [23] G. Ghiringhelli, *Resonant spectroscopies with circularly polarised soft x-rays*, Ph.D. thesis, Universit J. Fourier (2001).
- [24] M. Moretti Sala, V. Bisogni, C. Aruta, G. Balestrino, H. Berger, N. B. Brookes, G. M. De Luca, D. Di Castro, M. Grioni, M. Guarise, P. G. Medaglia, F. Miletto Granozio, M. Minola, P. Perna, M. Radovic, M. Salluzzo, T. Schmitt, K. J. Zhou, L. Braicovich, and G. Ghiringhelli, *New Journal of Physics* **13**, 043026 (2011).
- [25] B. Andlauer, J. Schneider, and W. Tolksdorf, *Physica Status Solidi B* **73**, 533 (1976).
- [26] N. A. Bogdanov, V. M. Katukuri, H. Stoll, J. van den Brink, and L. Hozoi, *Phys. Rev. B* **85**, 235147 (2012).
- [27] C. Rayan Serrao, J. Liu, J. T. Heron, G. Singh-Bhalla, A. Yadav, S. J. Suresha, R. J. Paull, D. Yi, J.-H. Chu, M. Trassin, A. Vishwanath, E. Arenholz, C. Frontera, J. Železný, T. Jungwirth, X. Marti, and R. Ramesh, *Phys. Rev. B* **87**, 085121 (2013).
- [28] J. Nichols, J. Terzic, E. G. Bittle, O. B. Korneta, L. E. D. Long, J. W. Brill, G. Cao, and S. S. A. Seo, *Applied Physics Letters* **102**, 141908 (2013).